The Plant Cell, Vol. 20: 589–601, March 2008, www.plantcell.org

EMB2473/MIRO1, an *Arabidopsis* Miro GTPase, Is Required for Embryogenesis and Influences Mitochondrial Morphology in Pollen [W]

Shohei Yamaoka[1] and Christopher J. Leaver[2]

Department of Plant Sciences, University of Oxford, Oxford OX1 3RB, United Kingdom

The regulation of mitochondrial biogenesis, subcellular distribution, morphology, and metabolism are essential for all aspects of plant growth and development. However, the molecular mechanisms involved are still unclear. Here, we describe an analysis of the three *Arabidopsis thaliana* orthologs of the evolutionarily conserved Miro GTPases. Two of the genes, *MIRO1* and *MIRO2*, are transcribed ubiquitously throughout the plant tissues, and their gene products localize to mitochondria via their C-terminal transmembrane domains. While insertional mutations in the *MIRO2* gene do not have any visible impact on plant development, an insertional mutation in the *MIRO1* gene is lethal during embryogenesis at the zygote to four-terminal-cell embryo stage. It also substantially impairs pollen germination and tube growth. Laser confocal and transmission electron microscopy revealed that the *miro1* mutant pollen exhibits abnormally enlarged or tube-like mitochondrial morphology, leading to the disruption of continuous streaming of mitochondria in the growing pollen tube. Our findings suggest that mitochondrial morphology is influenced by MIRO1 and plays a vital role during embryogenesis and pollen tube growth.

INTRODUCTION

Mitochondria are the main sites for aerobic energy production and supply various intermediates necessary for cellular metabolism. They are also involved in cellular processes, including the defense response against oxidative stress, calcium signaling, and the regulation and execution of programmed cell death (reviewed in Logan, 2006a; McBride et al., 2006). Thus, the coordination and regulation of mitochondrial biogenesis and function are vital during plant growth and development from zygote to mature plant. In addition, molecular mechanisms also exist to ensure that mitochondria are equally segregated between daughter cells during cell division and are properly distributed in cells undergoing rapid morphological differentiation and metabolic change. Such mechanisms are particularly important in plants, in which mitochondrial function and morphology must adapt in response not only to intracellular signals regulating plant development and differentiation but also to constantly changing external environmental conditions and biotic stresses.

In other eukaryotes, it has been shown that mitochondrial fusion and fission rely on evolutionarily conserved dynamin-like GTPases and their binding partners (reviewed in Yaffe, 1999; Okamoto and Shaw, 2005; Chan, 2006b), while mitochondrial motility is dependent on the cytoskeletal network (reviewed in Hollenbeck, 1996; Yaffe, 1999; Hollenbeck and Saxton, 2005; Boldogh and Pon, 2006, 2007; Frederick and Shaw, 2007). Dysfunction of these dynamic processes often causes developmental defects and diseases in mammals and insects (reviewed in Chan, 2006a, 2006b). Loss of the dynamin-like GTPases required for mitochondrial fusion causes embryonic lethality in mice (Chen et al., 2003) and neurodegenerative diseases in humans (Alexander et al., 2000; Delettre et al., 2000; Züchner et al., 2004). In *Drosophila*, severe loss of mitochondria in synaptic termini and impaired neurotransmission are caused by disruption of the axonal transport machinery of mitochondria (Stowers et al., 2002; Guo et al., 2005).

Our understanding of the molecular machinery that regulates mitochondrial morphology and motility in plants is still at an early stage (reviewed in Logan, 2006b). It has been shown that mitochondrial fission requires the dynamin-like GTPases (Arimura and Tsutsumi, 2002; Arimura et al., 2004a; Fujimoto et al., 2004; Logan et al., 2004). Although frequent fusion events have been demonstrated using fluorescent reporter proteins (Arimura et al., 2004b; Sheahan et al., 2005), the genes mediating mitochondrial fusion have not been identified. The motility of mitochondria is dependent mainly on actin filaments (Van Gestel et al., 2002) and is vital for proper mitochondrial inheritance (Barr et al., 2005) and during cell division (Sheahan et al., 2004). Changes in mitochondrial morphology and motility are associated with cell growth (Sheahan et al., 2004, 2005), senescence (Zottini et al., 2006), cell death induced by reactive oxygen species (Yoshinaga et al., 2005), and various physiological responses (Stickens and

[1] Current address: Ishikawa Prefectural University, 1-308 Suematsu, Nonoichi, Ishikawa 921-8836, Japan.
[2] Address correspondence to chris.leaver@plants.ox.ac.uk.
The author responsible for distribution of materials integral to the findings presented in this article in accordance with the policy described in the Instructions for Authors (www.plantcell.org) is: Christopher J. Leaver (chris.leaver@plants.ox.ac.uk).
[W] Online version contains Web-only data.
www.plantcell.org/cgi/doi/10.1105/tpc.107.055756

Verbelen, 1996; Armstrong et al., 2006), implying an important role in developmental processes and physiological function in plants.

A novel class of GTPases, the Miro GTPase family, was recently identified in humans (Fransson et al., 2003, 2006), mice (Shan et al., 2004), yeast (Frederick et al., 2004), and *Drosophila* (Guo et al., 2005). They contain two GTPase domains and two calcium binding EF-hand motifs and are associated with the outer mitochondrial membrane via their C-terminal transmembrane domains (TMs) (Figure 1A). The overexpression of human Miro GTPases containing wild-type and mutated functional domains leads to aggregated or thread-like mitochondrial morphology (Fransson et al., 2003, 2006). In the budding yeast *Saccharomyces cerevisiae*, loss of the Miro GTPase induces pleiotropic effects on mitochondrial morphology, including swollen and tubule-like structures (Frederick et al., 2004). Loss of the *Drosophila* Miro GTPase causes a dysfunction of the axonal mitochondrial transport, leading to abnormal subcellular distribution of mitochondria in neurons and muscles, with the result that mutant larvae do not accumulate mitochondria at the synaptic termini and thus exhibit abnormal locomotion and premature lethality (Guo et al., 2005).

In this study, we have shown that the *Arabidopsis thaliana* genome contains three genes encoding putative Miro-related GTPases, that two of the genes, *MIRO1* and *MIRO2*, are transcribed throughout the plant tissues, and that their gene products localize to mitochondria. While mutations in the *MIRO2* gene do not have any obvious impact on plant development, a mutation in the *MIRO1* gene leads to an arrest of embryogenesis at an early stage and substantially impairs pollen germination and tube growth. Microscopic analysis and live-cell imaging revealed that the *miro1* mutation causes abnormal mitochondrial morphology, leading to the disruption of continuous streaming of mitochondria in growing pollen tubes. Our data suggest that proper mitochondrial morphology influenced by MIRO1 is essential for embryogenesis and pollen tube growth in *Arabidopsis*.

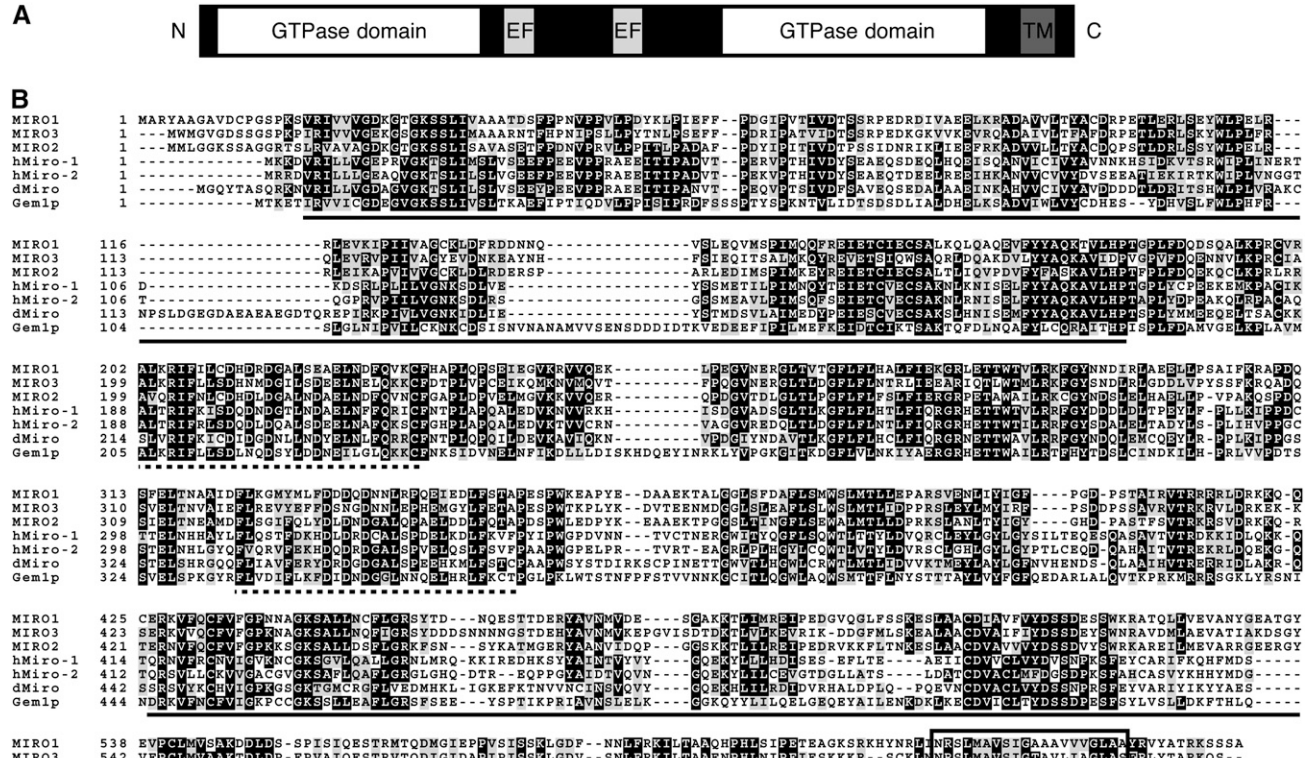

Figure 1. Alignment of the Predicted Amino Acid Sequences of Miro GTPases.

(A) Schematic diagram of the predicted protein structure of the Miro GTPases. EF, EF hand motif.

(B) Alignment of the predicted amino acid sequences of *Arabidopsis* (MIRO1, -2, and -3), human (hMiro-1 and -2), *Drosophila* (dMiro), and yeast (Gem1p) Miro GTPases. Black boxes indicate identical amino acid residues, gray boxes indicate conserved amino acid substitutions, solid underlines indicate the GTPase domains, dotted underlines indicate the EF-hand motifs, and the black open box indicates the TM. Sequences were aligned using the default settings in ClustalW version 1.81 (Thompson et al., 1994) and shaded using BOXSHADE 3.21 (http://ch.embnet.org/software/BOX_form.html).

RESULTS

The *Arabidopsis* Genome Contains Three Miro-Related GTPase Genes

Three orthologous genes of the Miro GTPase, *MIRO1* (At5g27540; also known as *EMB2473*) (Tzafrir et al., 2004), *MIRO2* (At3g63150), and *MIRO3* (At3g05310), were identified in a basic BLAST search (Altschul et al., 1997) of the *Arabidopsis* cDNA database (www.Arabidopsis.org/Blast; Arabidopsis Genome Initiative, 2000) using the human Miro-1 (Fransson et al., 2003) as a query sequence. They shared 36, 38, and 33% amino acid identity with human Miro-1, respectively, and each contained a putative GTPase domain in the N-terminal region followed by a pair of EF-hand motifs and a second distinct GTPase domain. Single TMs were also predicted at their C termini (Figures 1A and 1B). In previous studies, the C-terminal TM was shown to be responsible for anchoring Miro GTPases onto the outer mitochondrial membrane in yeast (Frederick et al., 2004) and humans (Fransson et al., 2006).

RT-PCR analysis of all three *Arabidopsis* Miro-related genes revealed that *MIRO1* and *MIRO2* are expressed in seedlings, flowers, siliques, stems, mature and senescent rosette leaves, and roots, whereas *MIRO3* transcripts were not amplified in any of these tissues (see Supplemental Figure 1 online). Further assessment was done by reference to the *Arabidopsis* microarray gene expression database GENEVESTIGATOR (https://www.genevestigator.ethz.ch/; Zimmermann et al., 2004), which revealed that *MIRO1* and *MIRO2* are ubiquitously expressed in all plant tissues, and therefore presumably have a vital role, whereas the expression of *MIRO3* is almost undetectable (Figure 2).

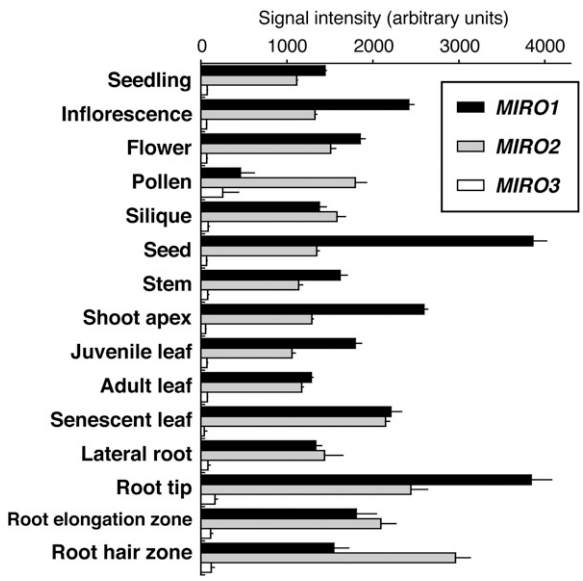

Figure 2. Gene Expression of the *Arabidopsis* Miro-Related GTPase Family in Various Plant Tissues.

Data used for the analysis were retrieved from GENEVESTIGATOR (Zimmermann et al., 2004). The values shown are means + SD.

The C-Terminal TM Is Required for Mitochondrial Localization of MIRO1 and MIRO2

Transient expression of cDNA constructs (GFP-MIRO1TM and GFP-MIRO2TM) containing the putative C-terminal TMs of MIRO1 (amino acid residues 602 to 648) and MIRO2 (amino acid residues 599 to 643) fused to the C terminus of an enhanced green fluorescent protein (GFP) in tobacco (*Nicotiana tabacum*) leaf epidermal cells showed colocalization with mitochondria labeled with the mitochondria-specific probe MitoTracker Orange ($n = 150$) (Figure 3). By contrast, C-terminal TM-deleted mutant proteins of MIRO1 (GFP-MIRO1ΔTM) and MIRO2 (GFP-MIRO2ΔTM) were excluded from mitochondria and dispersed throughout the cytosol ($n = 150$) (Figure 3). These results suggest that the C-terminal TM is required for mitochondrial localization of MIRO1 and MIRO2.

Embryogenesis Is Arrested at an Early Stage in the *miro1* Mutant

To investigate the role of *Arabidopsis* Miro-related GTPase genes during plant development, we identified *Arabidopsis* mutant lines from the public mutant collections. The *miro1* mutant, previously designated *emb2473*, was obtained from the SeedGenes Project collection (www.seedgenes.org; Tzafrir et al., 2004). The *miro1* mutant was generated by the introduction of pCSA110 T-DNA, which carries a BASTA resistance gene and a β-glucuronidase (GUS) reporter gene under the control of the pollen-specific *LAT52* promoter, into *Arabidopsis* plants harboring the homozygous *quartet1* (*qrt1*) mutation, which causes mature fertile pollen grains to remain attached to each other (Preuss et al., 1994; McElver et al., 2001). Sequence analysis revealed that the T-DNA was inserted at the border of the 12th intron and 13th exon of the *MIRO1* gene with a 16-bp deletion (Figure 4A). DNA gel blot analysis demonstrated that the T-DNA insertion was present as a single copy in the *miro1* mutant genome (see Supplemental Figure 2 online). Segregation analysis of the self-fertilized *miro1* progeny demonstrated that 54% of the progeny were resistant to BASTA, instead of the expected value of 75% (Table 1), implying embryonic and/or gametophytic lethality of the *miro1* mutant. PCR analysis revealed that a similar percentage (51%; $n = 112$) of the randomly selected progeny and all of the BASTA-resistant mutant progeny tested ($n = 50$) carried the T-DNA insertion, suggesting that the BASTA resistance and T-DNA insertion of the *miro1* mutant are tightly linked. No homozygous mutant plants were found, suggesting that the homozygous *miro1* mutant causes seed lethality.

We obtained two mutant lines, *miro2-1* and *miro2-2*, harboring T-DNA insertions in the 14th and 12th exon of the *MIRO2* gene, respectively, from the SALK collection (Alonso et al., 2003). Segregation analysis (see Supplemental Table 1 online) of the heterozygous mutant progeny suggested single T-DNA insertions in both the *miro2-1* and *miro2-2* mutants. Neither of the homozygous mutant progeny accumulated the full-length *MIRO2* transcripts (see Supplemental Figure 3 online). The phenotypes (see Supplemental Figure 4 online) and root cell mitochondrial morphology of both were indistinguishable from those of wild-type plants (see Supplemental Figure 5 online). These findings

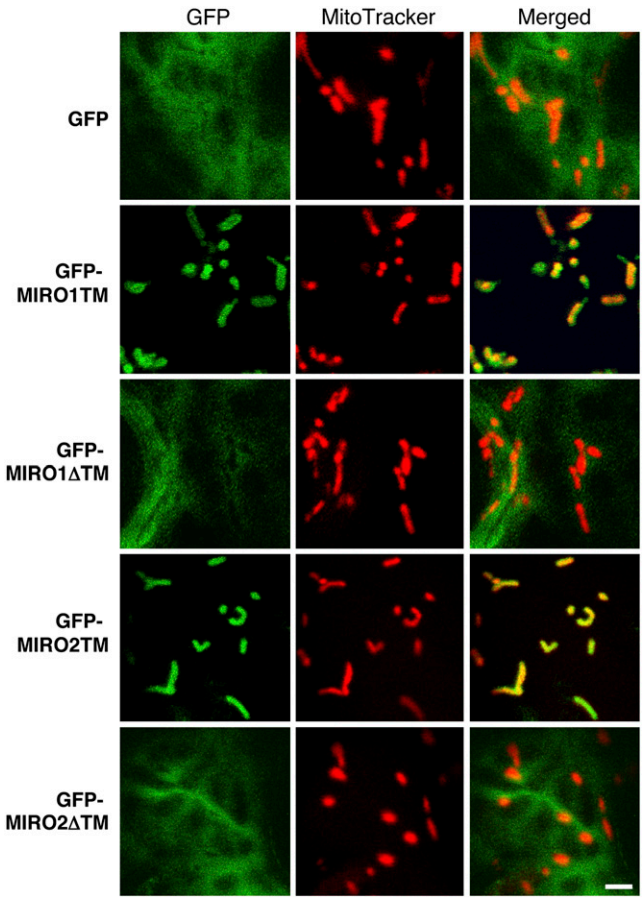

Figure 3. The C-Terminal TM Is Required for Mitochondrial Localization of MIRO1 and MIRO2.

Confocal images of GFP fluorescence (GFP), MitoTracker Orange staining (MitoTracker), and their merged images (Merged) are shown from tobacco leaf epidermal cells transiently expressing the indicated constructs. Bar = 2 μm.

suggest that *MIRO2* does not have a major role in plant development and does not share redundant functions with *MIRO1*; therefore, we concentrated our further analysis on the *miro1* mutant.

To investigate the developmental basis of the lethal phenotype displayed by the *miro1* mutant, maturing siliques from wild-type and heterozygous *miro1* mutant plants were dissected. The siliques from homozygous *qrt1* plants used as the wild-type control contained a well-ordered array of maturing green seeds (Figure 5A). By contrast, the siliques from heterozygous *miro1* mutant plants contained a proportion of aborted white seeds together with wild-type green seeds (Figure 5B). The white aborted seeds then turned brown and did not develop further, while the wild-type seeds developed to maturity (data not shown). More than 500 BASTA-resistant progeny of the *miro1* mutant displayed the aborted seed phenotype, suggesting that this mutant phenotype is tightly linked to BASTA resistance and the T-DNA insertion. Together, these findings suggest that the homozygous *miro1* mutation causes embryo lethality. However, the percentage of aborted seeds in the mutant siliques was significantly lower (13%; $n = 3154$) than the expected value of 25%, implying impaired pollen tube growth in the *miro1* mutant (Meinke, 1982).

To identify the developmental stage at which embryo development was arrested in the *miro1* mutant, immature seeds from heterozygous *miro1* mutant siliques were examined by whole-mount clearing and differential interference contrast (DIC) microscopy. A comparison of embryo development in normal seeds (Figures 5C and 5E to 5G) and aborted seeds (Figures 5D and 5H to 5L) revealed that embryogenesis was arrested at the early developmental stages between the zygote and the four-terminal-cell stage in the *miro1* mutant. Of the 80 mutant embryos examined, 8 embryos (10%) did not develop beyond the zygote (Figure 5I), 61 embryos (76%) aborted at the two-cell stage (Figures 5H and 5J), 7 embryos (9%) aborted at the three-cell stage (Figure 5K), and 4 embryos (5%) aborted at the four-terminal-cell stage (Figure 5L). These observations indicate that the homozygous *miro1* mutation causes abortion of the embryo at an early stage of development.

Pollen Germination and Tube Growth Are Impaired in the *miro1* Mutant

The abnormal segregation of selfed *miro1* mutant progeny (Table 1) and the lower than expected number of aborted seeds in the mutant siliques suggested that, in addition to the embryo

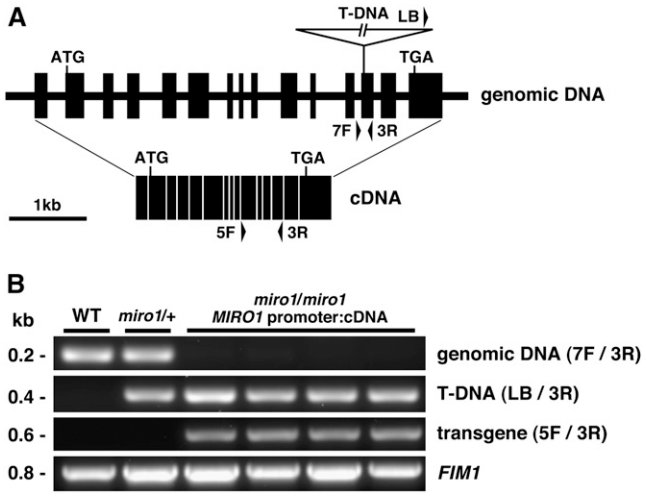

Figure 4. Gene Complementation of the *miro1* Mutant Using the *MIRO1* cDNA under the Control of Its Endogenous Promoter.

(A) Schematic diagram of *MIRO1* gene structure and the T-DNA insertion site in the *miro1* mutant. Closed boxes indicate exons, and closed arrowheads indicate the positions of primers used for genotyping. The start and stop codons are labeled.

(B) Gene complementation of the *miro1* mutant. All of the plants examined carried the homozygous *qrt1* background. For homozygous *miro1* plants complemented with the transgene (*MIRO1* promoter:cDNA), four independent lines were analyzed by genomic PCR amplification. PCR product sizes are indicated at left.

Table 1. Segregation and Genetic Transmission of the *miro1* Mutation

Cross (Female × Male)	BASTA^R	BASTA^S	BASTA^R/Total	TE (Female)	TE (Male)
miro1/+ × *miro1*/+	1480	1259	54.0%	NA	NA
miro1/+ × +/+	215	286	42.9%	75.2%	NA
+/+ × *miro1*/+	75	588	11.3%	NA	12.8%

Transmission efficiency (TE) was calculated according to Howden et al. (1998). BASTA^R, phosphinothricin-resistant; BASTA^S, phosphinothricin-sensitive; NA, not applicable; TE, BASTA^R/BASTA^S × 100.

lethality, genetic transmission through the gametophytes also was impaired. Reciprocal crosses with wild-type plants as the female parent demonstrated severely impaired male genetic transmission in the heterozygous *miro1* mutant (Table 1), suggesting that the *miro1* mutation strongly affects pollen development and/or germination and tube growth. If this is the case, the apical half region of the mutant silique should display a significantly higher percentage of aborted seeds than the expected 50% (Meinke, 1982). Indeed, 84% of the aborted seeds were located in the apical half regions of the *miro1* mutant siliques (n = 408). Additionally, the female genetic transmission of the *miro1* mutant was reduced slightly (Table 1), suggesting that the *miro1* mutation has a weak impact on female gametogenesis. This finding was supported by the fact that the frequency of unfertilized ovules was slightly higher in *miro1* mutant siliques (10%; n = 1254) than in wild-type siliques (4%; n = 1288).

The homozygous *qrt1* background causes mature fertile pollen grains to remain attached to each other and thus enables tetrad analysis to be performed (Preuss et al., 1994). Accordingly, the pollen tetrads from a heterozygous *miro1* mutant with the genotype *qrt1*/*qrt1*;+/*miro1* should contain two mutant and two wild-type pollen grains. However, the four grains were indistinguishable from each other in terms of their size and shape (Figure 6A). 4′,6-Diamidino-2-phenylindole (DAPI) and fluorescein diacetate (FDA) staining demonstrated that all four of the grains showed correctly differentiated one vegetative and two sperm nuclei (Figure 6B) and equal viability (Figure 6C). These findings suggest that *miro1* mutant pollen development is normal and thus does not explain the impaired male genetic transmission.

The *LAT52* promoter:GUS pollen-specific reporter gene contained in the pCSA110 T-DNA (McElver et al., 2001) makes it possible to distinguish between the *miro1* mutant and wild-type pollen by staining for GUS activity. To assess pollen viability in the *miro1* mutant, pollen from wild-type and heterozygous *miro1* mutant plants were germinated and stained in 5-bromo-4-chloro-3-indolyl-β-D-glucuronide (X-Gluc) solution, and the

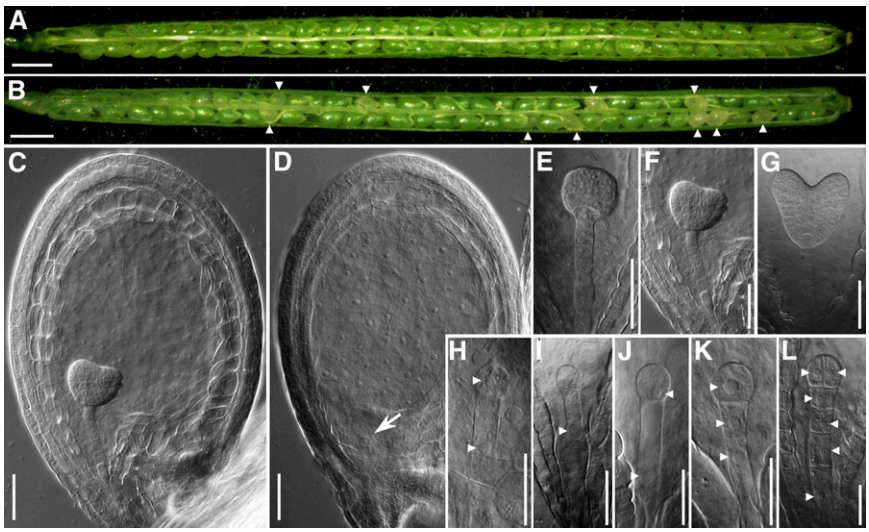

Figure 5. The Homozygous *miro1* Mutant Is Embryo-Lethal.

(A) and **(B)** Siliques from wild-type **(A)** and heterozygous *miro1* **(B)** plants. Arrowheads indicate the aborted mutant seeds. Bars = 1 mm.
(C) to **(L)** DIC images of seeds from heterozygous *miro1* mutant siliques.
(C) Wild-type seed containing a transition-stage embryo. Bar = 25 μm.
(D) and **(H)** *miro1* mutant seed containing a two-cell-stage embryo (arrow) **(D)**. A higher magnification of the mutant embryo exhibiting differentiated cell nuclei (arrowheads) is shown in **(H)**. Bars = 25 μm in **(D)** and 10 μm in **(H)**.
(E) to **(G)** Wild-type embryos: globular stage **(E)**, transition stage **(F)**, and heart stage **(G)**. Bars = 25 μm.
(I) to **(L)** *miro1* mutant embryos: zygote **(I)**, two-cell stage **(J)**, three-cell stage **(K)**, and four-terminal-cell stage **(L)**. Arrowheads indicate the mutant embryo nuclei. Bars = 10 μm.

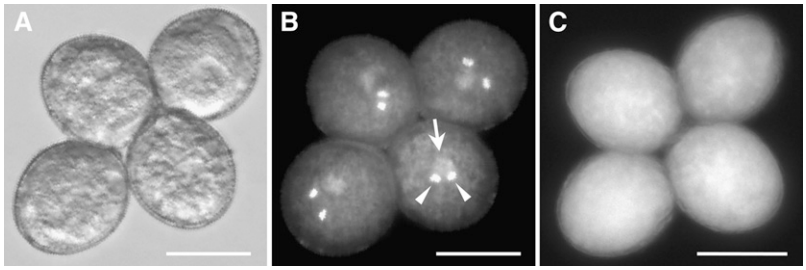

Figure 6. Pollen Development in the *miro1* Mutant Is Normal.

Mature pollen tetrads from heterozygous *miro1* plants (*qrt1*/*qrt1*;*miro1*/+): phase-contrast image **(A)**, DAPI staining of DNA **(B)**, and FDA staining to show viability **(C)**. Note that DAPI staining shows two sperm cell nuclei (arrowheads) and one vegetative cell nucleus (arrow). Bars = 20 μm.

germination and tube growth efficiencies were compared (Figures 7A and 7B). The GUS-negative wild-type pollen showed normal tube growth, while the GUS-positive mutant pollen showed impaired germination and tube growth. Approximately 70% of the wild-type pollen as well as the GUS-negative wild-type pollen from the heterozygous *miro1* mutant germinated, and the average tube length reached was ~150 μm (Figure 7D). By contrast, the germination rate of the GUS-positive mutant pollen was decreased to ~40%, and tube growth was reduced as well (Figure 7D). These findings suggest that the *miro1* mutation severely impairs pollen germination and tube growth.

A Mutation in *MIRO1* Causes Abnormal Mitochondrial Morphology in Pollen

In order to investigate the role of *MIRO1* in regulating mitochondrial morphology and intracellular distribution, mitochondria were visualized in pollen by creating transgenic plants containing

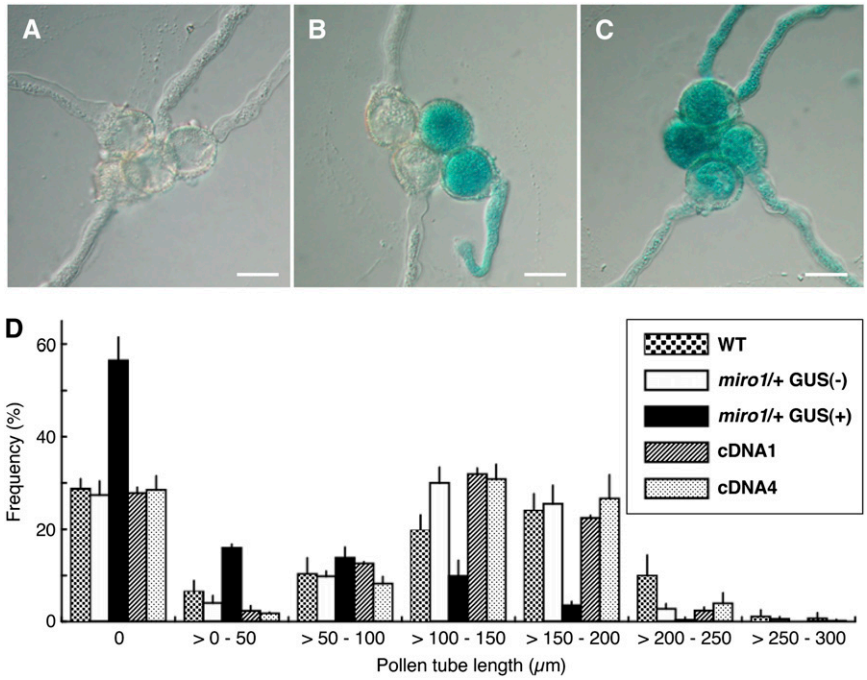

Figure 7. A Mutation in *MIRO1* Impairs Pollen Germination and Tube Growth.

(A) to **(C)** In vitro germination of pollen from wild-type (*qrt1*/*qrt1*;+/+) **(A)**, heterozygous *miro1* (*qrt1*/*qrt1*;*miro1*/+) **(B)**, and homozygous *miro1* (*qrt1*/*qrt1*;*miro1*/*miro1*) **(C)** plants complemented with the *MIRO1* promoter:cDNA. All were stained for GUS activity arising from the T-DNA inserted into the *MIRO1* locus. Bars = 20 μm.

(D) Pollen tube length from wild-type, heterozygous *miro1* (*miro1*/+), and two lines of homozygous *miro1* plants complemented with the *MIRO1* promoter:cDNA (cDNA1 and cDNA4). For heterozygous *miro1* plants, GUS-positive [GUS(+)] and GUS-negative [GUS(−)] pollen were scored separately. All of the plants examined carried the homozygous *qrt1* background. A failure to germinate is represented as zero pollen tube length. The means + SE of three independent experiments are shown ($n > 550$ for each line).

GFP fused to a mitochondrial targeting signal sequence (mtGFP) (Logan and Leaver, 2000) under the control of the pollen-specific *LAT52* promoter (Twell et al., 1990; Yang et al., 2001). Homozygous *qrt1* plants as the wild-type control were compared with heterozygous *miro1* mutant plants. Laser confocal microscopy revealed that all four pollen grains in the tetrads from control *qrt1* plants ($n = 50$) contained normal spherical or rod-like mitochondria (Figure 8A). By contrast, tetrads from heterozygous *miro1* mutant plants ($n = 50$) contained two pollen grains with normal mitochondrial morphology and two with abnormally enlarged mitochondria (Figure 8B). Following germination, using time-lapse confocal microscopy, we showed that in wild-type pollen ($n = 34$) mitochondria exhibited uniform rod-like morphology (Figure 8C) and high motility, leading to continuous streaming of mitochondria throughout the cytoplasm (Figure 8E; see Supplemental Movie 1 online). This motility is dependent on actin filaments, because disruption of actin filaments in pollen by latrunculin B or cytochalasin D (see Supplemental Figure 6A online) arrested mitochondrial motility (see Supplemental Movies 3 and 4 online), whereas disruption of microtubules by oryzalin or nocodazole (see Supplemental Figure 6B online) did not have any impact on the streaming of mitochondria (see Supplemental Movies 5 and 6 online). Mitochondria in the *miro1* mutant pollen ($n = 29$) exhibited an abnormal morphology and intracellular distribution (Figure 8D). In addition to the abnormal size (Figure 8F; time = 146 s), a large number of mitochondria also showed a tube-like morphology (Figure 8F; time = 49 s). These abnormal mitochondria were motile (see Supplemental Movie 2 online), often leading to transient absence from regions of the pollen cytoplasm (Figure 8F; time = 177 s). This motility was also actin-dependent (see Supplemental Movies 7 to 10 online), suggesting that the *miro1* mutation does not affect actin-dependent mitochondrial motility. Together, these observations suggest that the *miro1* mutation causes abnormally enlarged or tubulated mitochondrial morphology, leading to disruption of the continuous streaming of mitochondria in the growing pollen tube.

To investigate the detailed size and structures of their mitochondria, wild-type and *miro1* mutant pollen were germinated

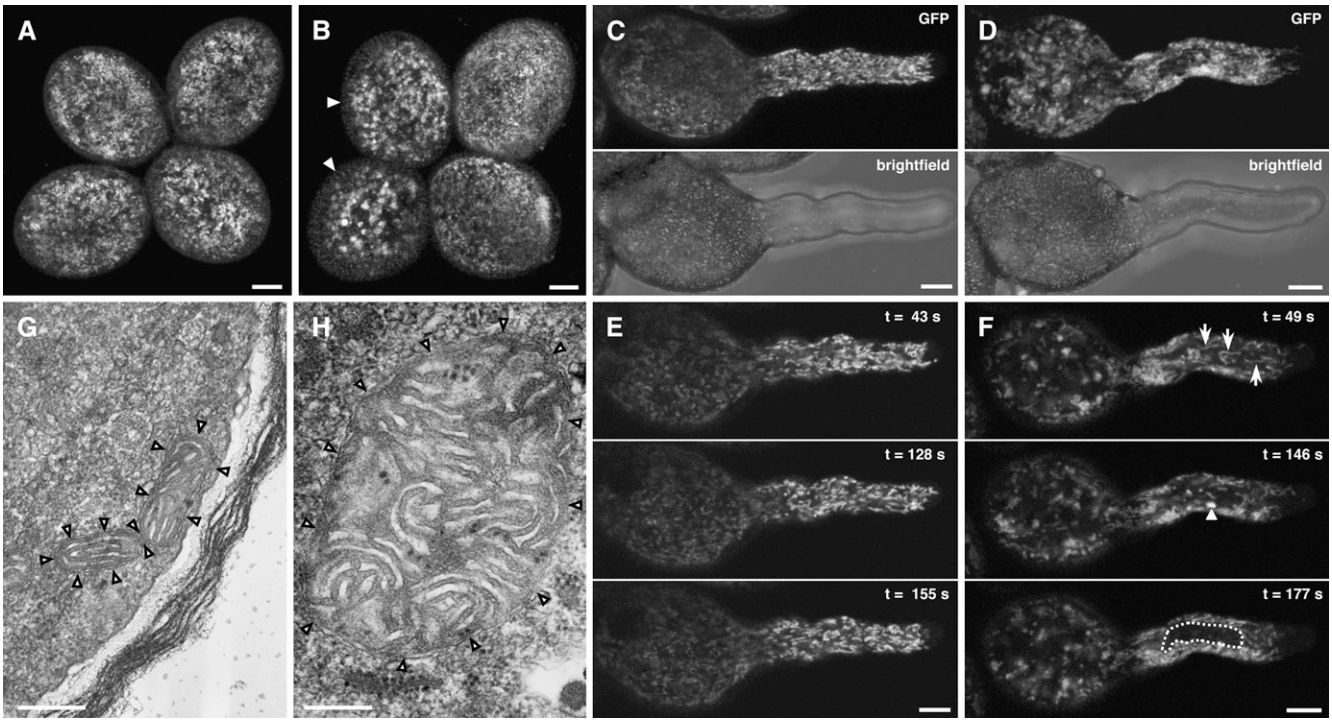

Figure 8. A Mutation in *MIRO1* Causes Abnormal Mitochondrial Morphology in Pollen.

(A) and **(B)** Merged confocal images of mitochondrial morphology and distribution in pollen tetrads labeled with mtGFP from wild-type (*qrt1*/*qrt1*;+/+) **(A)** and heterozygous *miro1* (*qrt1*/*qrt1*;*miro1*/+) **(B)** plants. Note that the two *miro1* mutant pollen grains (arrowheads in **[B]**) exhibit abnormally enlarged mitochondrial morphology. Bars = 5 μm.

(C) and **(D)** Merged confocal images of mitochondrial morphology and intracellular distribution in germinating wild-type **(C)** and *miro1* mutant **(D)** pollen. Top, GFP fluorescence; bottom, bright-field images. Bars = 5 μm.

(E) and **(F)** Time-lapse single confocal images of mitochondrial morphology and intracellular distribution in wild-type **(E)** and *miro1* mutant **(F)** pollen. t indicates the time point of the image in seconds from Supplemental Movies 1 and 2 online (**[E]** and **[F]**, respectively), in which mitochondrial movement can be seen. In **(F)**, arrows indicate abnormal mitochondria showing tube-like morphology, the arrowhead indicates abnormally enlarged mitochondria, and the dotted area indicates the absence of mitochondria in pollen cytoplasm. Bars = 5 μm.

(G) and **(H)** Transmission electron micrographs of mitochondria in wild-type **(G)** and *miro1* mutant **(H)** pollen. Open arrowheads indicate the outer mitochondrial membrane. Bars = 0.2 μm.

and visualized by transmission electron microscopy. The wild-type pollen contained rod-like mitochondria with an electron-dense matrix and well-developed inner membrane cristae (Figure 8G). The *miro1* mutant pollen contained much larger globular mitochondria (Figure 8H). These findings further support our suggestion that the abnormal mitochondrial morphology seen in *miro1* mutant pollen is due to the enlargement but not the aggregation of mitochondria.

MIRO1 cDNA Complements the *miro1* Mutant Phenotype

To confirm that the embryo lethality observed in the homozygous *miro1* mutant is caused by the insertional mutation in *MIRO1*, heterozygous *miro1* plants were transformed with a vector containing a *MIRO1* cDNA fused to the 1.7-kb genomic sequence 5′ upstream of the predicted translational start codon of the *MIRO1* gene (*MIRO1* promoter:cDNA) and the kanamycin-resistant marker gene. Three pairs of primers were designed to amplify the wild-type locus, the *miro1* mutant locus containing the inserted T-DNA, and the transgene (Figure 4A). Control PCR amplifications showed that the primer pairs were able to amplify the wild-type and mutant loci but not the transgene in the heterozygous *miro1* plants (Figure 4B). PCR screening of the kanamycin-resistant T1 plants with these primer pairs allowed us to identify four independent lines that were homozygous for the *miro1* mutant locus and harbored the transgene (Figure 4B). This result demonstrated that the embryo lethality observed in the homozygous *miro1* mutant was complemented by the *MIRO1* promoter:cDNA transgene.

Two of the homozygous *miro1* mutant lines (cDNA1 and cDNA4) harboring the transgene were assessed for pollen viability. The T3 plants from these lines produced pollen tetrads in which all four grains were GUS-positive (Figure 7C), germinated, and exhibited normal tube growth (Figure 7D). The mitochondrial morphology in these pollen tetrads was indistinguishable from that of wild-type plants (see Supplemental Figure 7 online). These results confirm that the *MIRO1* transgene reversed the impaired pollen viability and aberrant mitochondrial morphology seen in the *miro1* mutant. Together, these data confirm that expression of *MIRO1* cDNA under the control of the endogenous promoter complements the *miro1* mutant phenotype, namely embryo lethality and impaired pollen germination and tube growth.

DISCUSSION

Identification of *Arabidopsis* Miro-Related GTPases

Mitochondria are dynamic organelles that frequently change their morphology and intracellular distribution by various processes, including fission, fusion, and motility. Recent studies have revealed that plants are likely to share similar machinery for the regulation of mitochondrial morphology and motility with other eukaryotic organisms (reviewed in Logan, 2006b). In various organisms, the Miro GTPases were identified recently as novel mitochondria-localized GTPases that are involved in the regulation of mitochondrial morphology and intracellular distribution (Fransson et al., 2003, 2006; Frederick et al., 2004; Guo et al., 2005). Using the predicted human protein sequence, we identified three orthologs of the Miro GTPase encoded in the *Arabidopsis* genome. The predicted protein structures of these orthologs are highly conserved among the species (Figure 1), and we have shown that two of the genes, *MIRO1* and *MIRO2*, encode proteins that localize to mitochondria via their C-terminal TMs (Figure 3), suggesting that they share similar functions with the previously characterized Miro GTPases.

Gene expression analysis revealed that *MIRO1* and *MIRO2* are expressed in all tissues examined (Figure 2), suggesting that they are functional in *Arabidopsis*. However, while a mutation in *MIRO1* has a severe impact on mitochondrial morphology (Figure 8) and causes embryo lethality (Figure 5) and impaired pollen germination and tube growth (Figure 7), insertional mutations in *MIRO2* do not have any impact on mitochondrial morphology (see Supplemental Figure 5 online) and show no obvious effects on plant development (see Supplemental Figure 4 online). These findings suggest that *MIRO1* and *MIRO2* are not functionally redundant but, rather, that *MIRO1* has a major role in the regulation of mitochondrial morphology during the reproductive process and subsequent embryo development. The role of *MIRO1* in later developmental stages was not examined in this study because of the homozygous lethality of the insertional mutation. It could be investigated in the future using another experimental system, for example, by creating transgenic plants that enable the inducible control of *MIRO1* expression.

MIRO1 Is Required for Embryogenesis and Pollen Tube Growth

Mutations in the genes involved in the regulation of morphology and intracellular distribution of mitochondria often cause developmental defects and human genetic disease, indicating that mitochondrial morphology and distribution are indispensable for animal development (reviewed in Chan, 2006b). In plants, however, the identities of the genes influencing mitochondrial morphology and distribution are not known, and neither are their effects on development. In this study, we have demonstrated that *MIRO1* is required for embryogenesis and pollen viability and function in *Arabidopsis*.

Analysis of an insertional mutant of the *MIRO1* gene revealed that it was not possible to recover homozygous mutant plants. The siliques from the heterozygous mutant plants contained a significant proportion of aborted seeds (Figure 5B), suggesting that the homozygous *miro1* mutation causes embryo lethality. Most of the aborted seeds contained two-cell-stage embryos (Figures 5D, 5H, and 5J), indicating that the homozygous *miro1* mutation severely inhibits embryonic cell division. The *Arabidopsis* zygote undergoes polarized cell elongation after fertilization and the subsequent asymmetric division to produce the apical and basal cells. The elongating zygote accumulates mitochondria in its apical region, whereas the cytoplasmic density of mitochondria remains uniform in the subsequent apical cell division (Mansfield and Briarty, 1990), implying that precise regulation of mitochondrial distribution is required for the progress of embryogenesis. Miro GTPases are known to be involved in regulating mitochondrial morphology and distribution in various organisms (Fransson et al., 2003, 2006; Frederick et al., 2004; Guo et al., 2005), and in this study, we demonstrated that

MIRO1 has a role in influencing mitochondrial morphology in pollen (Figure 8). Therefore, we propose that the intracellular distribution of mitochondria is regulated by *MIRO1* and is essential for the normal progress of embryo development.

We also observed that mutation in *MIRO1* severely reduced male genetic transmission (Table 1). Heterozygous *miro1* mutant plants produced siliques in which the apical half contains a significantly higher number of aborted seeds than expected, suggesting that pollen development or function is impaired in the *miro1* mutant (Meinke, 1982). Microscopic analysis and in vitro germination assays revealed that a mutation in *MIRO1* does not affect pollen development (Figure 6) but impairs pollen germination and tube growth (Figure 7). Approximately 60% of *miro1* mutant pollen grains did not germinate, although the remainders were capable of initiating tube growth. However subsequent tube growth was impaired significantly compared with the wild-type pollen, and <4% were capable of growing to >150 μm in length (Figure 7D). These findings suggest that *MIRO1* is required for normal pollen germination and tube growth.

It has been reported that during pollen tube growth mitochondria exhibit continuous streaming in the cytoplasm (Parton et al., 2003; Lovy-Wheeler et al., 2007). Miro GTPases have been shown to be involved in the regulation of mitochondrial morphology and distribution in various organisms; therefore, we postulated that *MIRO1* may be required for proper mitochondrial streaming during pollen germination and tube growth. In order to investigate this, we visualized mitochondria by confocal microscopy of the wild-type and *miro1* mutant pollen from transgenic plants containing mtGFP under the control of the pollen-specific *LAT52* promoter. While uniform morphology (Figures 8A and 8C) and continuous streaming of mitochondria (Figure 8E; see Supplemental Movie 1 online) were observed in wild-type pollen, *miro1* mutant pollen exhibited abnormal morphology (Figures 8B, 8D, 8F) and disrupted streaming of mitochondria (Figure 8F; see Supplemental Movie 2 online), including transient absences from regions of the cytoplasm (Figure 8F; time = 177 s). Pollen germination and tube growth involve a significant number of energy- and metabolite-dependent cellular processes, including cell wall synthesis and vesicular trafficking, specifically in the apical region of the tube (reviewed in Krichevsky et al., 2007). The disruption of streaming and the abnormal morphology of mitochondria in *miro1* mutant pollen may result in reduced energy and metabolite supply to those cytoplasmic regions where such cellular processes are vital for pollen germination and tube growth.

MIRO1 Is Involved in the Regulation of Plant Mitochondrial Morphology

Pollen-specific expression of mtGFP revealed that a *miro1* mutation leads to abnormally enlarged or tube-like mitochondria (Figure 8). This finding suggests that MIRO1 plays a role in the regulation of mitochondrial morphology and that the mutation in *MIRO1* may cause increased fusion and/or decreased fission of mitochondria. Similar observations have been reported in the analysis of *GEM1*, a single-copy gene encoding a Miro GTPase in the budding yeast. Loss of *GEM1* leads to a pleiotropic defect in mitochondrial morphology, including swollen and tube-like structures (Frederick et al., 2004). These data suggest that Miro GTPases may play a role in regulating mitochondrial fusion/fission events in both budding yeast and plants. However, Gem1p is not associated directly with the mitochondrial fusion/fission machineries reported previously, suggesting that Miro GTPases may be involved in a novel pathway for regulating mitochondrial morphology (Frederick et al., 2004).

Recent studies in *Drosophila* suggested the involvement of a Miro GTPase in mitochondrial transport in the neural axon (Guo et al., 2005). The *Drosophila* Miro GTPase associated with a 120-kD protein, designated Milton, to form a protein complex that bound to the kinesin heavy chain, leading to the recruitment of mitochondria to microtubules (Glater et al., 2006). The human Miro GTPases also are associated with two Milton orthologs, GRIF-1 and OIP106, which interact with kinesin and mitochondria (Brickley et al., 2005; Fransson et al., 2006). These studies suggest that the Miro GTPase may be a component of the microtubule-dependent transport machinery of mitochondria (Glater et al., 2006; Rice and Gelfand, 2006; Frederick and Shaw, 2007). Our study demonstrated that mitochondria motility in pollen is actin-dependent and not likely to be affected by the *miro1* mutation (see Supplemental Movies 3 to 12 online). We also failed to identify any obvious ortholog of *Drosophila* Milton in *Arabidopsis* by a basic BLAST search of the cDNA database (data not shown). These observations suggest that, similar to yeast Gem1p (Frederick et al., 2004; Rice and Gelfand, 2006; Boldogh and Pon, 2007; Frederick and Shaw, 2007), MIRO1 plays a major role in influencing mitochondrial morphology and might interact with partner proteins that differ from human and *Drosophila* Miro GTPases. Future studies on the proteins interacting with MIRO1 may give further insight into the mechanism by which Miro GTPases regulate mitochondrial morphology in plants.

METHODS

Expression Analysis

Gene expression data were collected from the GENEVESTIGATOR website (www.genevestigator.ethz.ch; Zimmermann et al., 2004) with the default settings and processed using Microsoft Excel.

Subcellular Localization Assay

The partial cDNA sequences of *MIRO1* and *MIRO2* were amplified using *Arabidopsis thaliana* leaf cDNA (for preparation, see Supplemental Methods online) as template and primer pairs as follows: for MIRO1TM, 5′-TTAAGCGGCCGCTCAGGCAGACGAGCTCTT-3′ and 5′-AATTGGTACCAGGAGACCGAAGCAGGCAA-3′; for MIRO1ΔTM, 5′-AATTGGTACCAGATGGCGAGATACGCTGC-3′ and 5′-AATTGCGGCCGCTATGGAATGCTCAAATGAGG-3′; for MIRO2TM, 5′-AATTGGTACCAGGAGACAGAGTCAGGAAGAAGAAG-3′ and 5′-AATTGCGGCCGCTCAAGCATTCTTCCTTGC-3′; and for MIRO2ΔTM, 5′-ATGCGGTACCCGATGATGCTCGGTGGAAAG-3′ and 5′-AATTGCGGCCGCTATGGAATGCTCATGTGAGG-3′. Ten cycles of PCR were performed at 98°C for 10 s, 55°C for 5 s, and 72°C for 30 s or 2 min, followed by 20 cycles at 98°C for 10 s and 68°C for 30 s or 2 min. The PCR fragments were digested with *Kpn*I and *Not*I and ligated into the pENTR1a vector (Invitrogen). DNA inserts were transferred into pK7WGF2 (Karimi et al., 2005) by Gateway recombination (Invitrogen). *Agrobacterium tumefaciens* containing the resultant vectors was infiltrated into the

leaf epidermal cells of tobacco (*Nicotiana tabacum* cv SR1) seedlings grown at 21°C on soil under continuous light for 4 to 5 weeks (Batoko et al., 2000). Fluorescence was visualized at 30 to 35 h later. GFP fluorescence of the fusion proteins was excited at 488 nm with a 25-mW argon laser, and the emitted light was collected through a 475- to 525-nm filter and acquired using a Zeiss LSM 510 laser scanning confocal microscope with a 40× C-Apochromat water-immersion lens (numerical aperture = 1.2). Mitochondria were stained by infiltration of 200 nM MitoTracker Orange CMTMRos (Invitrogen) into the apoplastic space of tobacco leaves. The fluorescence of MitoTracker was excited at 543 nm with a HeNe laser, and the emitted light was collected through a 585- to 615-nm filter. Images were acquired as z-series with 3-μm intervals, merged, and processed using Zeiss LSM Examiner and Adobe Photoshop 7.0.

Mutant Lines and Growth Conditions

A mutant line in the SeedGenes Project collection, *emb2473*, and two Salk lines, SALK_060075 and SALK_151790 (background Columbia), were obtained from the Nottingham Arabidopsis Stock Centre and designated *miro1*, *miro2-1*, and *miro2-2*, respectively. The genotypes of these lines were confirmed by PCR amplification using gene-specific primers (for *miro1*, 5′-TCCTGCTGTTTGATTGGTTG-3′ and 5′-CTGGTGGATTCTTGTATGGA-3′; for *miro2-1*, 5′-ATCCGCCAACTCGTGAATAG-3′ and 5′-AGAAAAACATCAAGTGTTTTATTACTAAGT-3′; for *miro2-2*, 5′-GCGAGGGAAATACTGATGGA-3′ and 5′-TTCACGAGTTGGCGGATATT-3′) and T-DNA–specific primers (for *miro1*, 5′-GCCTTTTCAGAAATGGATAAATAGCCTTGCTTCC-3′; for *miro2-1* and *miro2-2*, 5′-TGGTTCACGTAGTGGGCCATCG-3′). The template DNA was prepared by the method of Neff et al. (1998). PCR was performed at 96°C for 1 min followed by 35 cycles at 96°C for 30 s, 57°C for 30 s, and 72°C for 1 min. Seeds were surface-sterilized and plated onto 0.8% (w/v) agar medium containing half-strength Murashige and Skoog salts (pH 5.8; Duchefa Biochemie), which were supplemented with 7.5 mg/L phosphinothricin or 30 mg/L kanamycin as required. The seeds were vernalized and germinated, and the 10-d-old seedlings were transferred onto soil and grown at 21°C under a 16-h-light/8-h-dark regime.

Histological Analysis

Characterization of the seed phenotype in siliques from homozygous *qrt* and heterozygous *miro1* plants was performed according to the protocol of Yadegari et al. (1994). Seeds were fixed and cleared in chloral hydrate solution, and the embryos were observed using a Zeiss Axioplan 2 microscope with DIC optics.

Cytological Analysis and in Vitro Germination Assay of Pollen

Cytological analysis of mature pollen grains was performed by incubating pollen in 1 μg/mL DAPI and 20 μM FDA solutions and visualization using a fluorescence microscope (Olympus BX50). The in vitro germination assays were performed by dipping mature flowers into 1% (w/v) agar medium containing germination buffer (50 mM MES, pH 5.8, 1 mM KCl, 10 mM $CaCl_2$, 0.8 mM $MgSO_4$, 0.01% [w/v] H_3BO_3, and 18% [w/v] sucrose) (Fan et al., 2001) after which the plates were sealed and incubated at 20°C for 8 to 9 h. Pollen grains were stained at 37°C overnight in 1 mM X-Gluc solution containing 50 mM Na_3PO_4, 0.5 mM $K_3Fe(CN)_6$, 0.5 mM $K_4Fe(CN)_6$, 0.01% (w/v) Triton X-100, 10 mM EDTA, and 18% (w/v) sucrose and then observed and scored with a Leica MZFLIII microscope. The pollen tube lengths were measured in the captured images using NIH Image version 1.63 (http://rsb.info.nih.gov/nih-image/).

Visualization of Mitochondria

Plant mitochondria were visualized in plants transformed with a vector containing *LAT52* promoter–tobacco etch virus translational enhancer (TEVL) sequence (Yang et al., 2001), tobacco mitochondrial β-ATPase signal sequence (Logan and Leaver, 2000), and the GFP sequence, which were amplified using pLAT52-TEVL GFP, pGEM-β-ATPase signal sequence:mGFP5, and pK7WGF2 as templates, respectively. Sequences of the primer pairs were as follows: for *LAT52* promoter–TEVL, 5′-GGGGACAACTTTGTATAGAAAAGTTGGTCGACATACTCGACTCAGAAGGTA-3′ and 5′-GGGGACTGCTTTTTTGTACAAACTTGGGCTATCGTTCGTAAATGGT-3′; for tobacco mitochondrial β-ATPase signal, 5′-GGGGACAAGTTTGTACAAAAAAGCAGGCTTCACCATGGCTTCTCGGAGGCTTCTC-3′ and 5′-GGGGACCACTTTGTACAAGAAAGCTGGGTTACCAGCGCCGGTGAACTCATCGGTA-3′; and for GFP, 5′-GGGGACAGCTTTCTTGTACAAAGTGGATATGGTGAGCAAGGGCGAGGA-3′ and 5′-GGGGACAACTTTGTATAATAAAGTTGCCGCGGTTACTTGTACAGCTCGTC-3′. Thirty-five cycles of PCR were performed at 98°C for 10 s, 55°C for 5 s, and 72°C for 1 min. The amplified sequences were transferred into the pK7m34GW vector (Karimi et al., 2005) using the MultiSite Gateway system (Invitrogen). The construct was introduced into the homozygous *qrt1* and heterozygous *miro1* mutant plants according to the method of Clough and Bent (1998), and three independent T2 plants were used for the microscopic analysis. Pollen grains from these transgenic plants were germinated on 1% (w/v) agar medium containing germination buffer poured on the slide glass and incubated at 20°C for 4 to 6 h. GFP fluorescence of pollen mitochondria was acquired using the confocal microscope as described above. Time-lapse imaging was performed with a series of single confocal images collected by scanning at 2- to 6-s intervals. Mitochondria were also visualized by staining plant materials with 200 nM MitoTracker Orange (Invitrogen). All images were processed using Zeiss LSM Examiner and Adobe Photoshop 7.0.

Transmission Electron Microscopy

Pollen grains from homozygous *qrt1* and heterozygous *miro1* plants were germinated on 1% (w/v) agar medium containing germination buffer for 2 h. Phosphate buffer (50 mM; pH 7.0) containing 4% (w/v) paraformaldehyde, 3% (w/v) glutaraldehyde, and 18% (w/v) sucrose was then poured onto the agar medium, and the plates were incubated at room temperature for 2 h. The surfaces of the agar plates were rinsed twice with 50 mM phosphate buffer containing 18% (w/v) sucrose and incubated for a further 2 h in 1% (w/v) osmium tetroxide. After rinsing with water, agar cubes carrying the germinated pollen grains were excised, dehydrated in a series of acetone solutions (25, 50, 75, and 100% [v/v]) followed by a resin/acetone dilution series (25, 50, and 75% [v/v]), and embedded in epoxy resin. Serial cross sections were examined with a JEOL JEM1010 transmission electron microscope and a Kodak Megaplus model 1.4 digital camera. Images were processed using Adobe Photoshop 7.0.

Cytoskeletal Inhibitor Experiments

Stock solutions of 1 mM latrunculin B, 10 mM cytochalasin D, 10 mM oryzalin, and 10 mM nocodazole were prepared in DMSO and diluted in germination buffer. Pollen grains were germinated on 1% (w/v) agar medium containing germination buffer for 4 to 6 h and excised as small agar blocks. They were incubated in germination buffer containing 1 μM latrunculin B, 10 μM cytochalasin D, 10 μM oryzalin, and 10 μM nocodazole for 30 min, then mitochondria were visualized as described above. Treatment with 0.1% (w/v) DMSO did not have any effect on mitochondrial motility in pollen (see Supplemental Movies 11 and 12 online).

Gene Complementation

The coding sequence of *MIRO1* cDNA and the 1.7-kb 5′ upstream sequence were amplified using *Arabidopsis* leaf cDNA and pBeloBAC clone F15A18 (Arabidopsis Genome Initiative, 2000) as templates, respectively.

Sequences for the primer pairs are as follows: for the coding sequence, 5′-AATTGGTACCAGATGGCGAGATACGCTGC-3′ and 5′-TTAAGC-GGCCGCTCAGGCAGACGAGCTCTT-3′; for the upstream sequence, 5′-AGGTGGATCCCTCTAAAGTGGTTGTGGTGG-3′ and 5′-GTACGG-TACCCTGAAACTGCAACACAATCA-3′. Thirty-five cycles of PCR were performed at 98°C for 10 s, 55°C for 5 s, and 72°C for 2 min. The PCR fragments were digested with *Kpn*I/*Not*I and *Bam*HI/*Kpn*I for *MIRO1* cDNA and the upstream sequence, respectively, and ligated into the *Bam*HI–*Not*I sites of pENTR1a vector (Invitrogen). The cauliflower mosaic virus 35S terminator sequence was amplified by 25 cycles of PCR at 98°C for 10 s, 55°C for 5 s, and 72°C for 30 s using the primers 5′-GCG-CGCACTAGTATGCTAGAGTCCGCAAAAAT-3′ and 5′-GCGCTTAAGCT-TGGTCACTGGATTTTGGTTTT-3′ and pK7WGF2 as template. The PCR fragment was digested and inserted into the *Spe*I–*Hin*dIII sites of pKGW (Karimi et al., 2005), and these two vectors were used to perform Gateway recombination (Invitrogen). The resultant construct (*MIRO1* promoter: cDNA) was confirmed by sequencing and introduced into heterozygous *miro1* plants according to the method of Clough and Bent (1998). The T1 plants were selected on 30 mg/L kanamycin, and plants homozygous for the *miro1* mutant locus were identified by PCR amplification. Sequences of the primers used were as follows: 5F, 5′-ACTGCCCTTGGAGGAC-TATC-3′, 7F, 5′-TCCTGCTGTTTGATTGGTTG-3′, 3R, 5′-CTGGTGGAT-TCTTGTATGGA-3′, and LB1, 5′-GCCTTTTCAGAAATGGATAAATAG-CCTTGCTTCC-3′. The positions of these primers are indicated in Figure 4. The primers specific for *FIM1* (At4g27600) (5′-TGACAAGG-TCTCTCCCAGTTC-3′ and 5′-GAACAACCGAGCTTTCTTGC-3′) were used for the positive control. The templates were prepared by the method of Neff et al. (1998), and PCR was performed at 96°C for 1 min followed by 35 cycles at 96°C for 30 s, 57°C for 30 s, and 72°C for 1 min. The T2 plants homozygous for both the *miro1* mutant locus and the transgene were identified by segregation analysis for kanamycin resistance, and the T3 plants were used for further analysis.

Accession Numbers

Arabidopsis Genome Initiative numbers for the genes mentioned in this study are as follows: *MIRO1*, At5g27540; *MIRO2*, At3g63150; *MIRO3*, At3g05310; *UBQ10*, At4g05320; and *FIM1*, At4g27600.

Supplemental Data

The following materials are available in the online version of this article.

Supplemental Figure 1. RT-PCR Analysis of the *MIRO* Genes.

Supplemental Figure 2. DNA Gel Blot Analysis of the *miro1* Mutant.

Supplemental Figure 3. Identification of *miro2* Mutants.

Supplemental Figure 4. Phenotypes of Homozygous *miro2* Mutants Are Indistinguishable from Those of Wild-Type Plants.

Supplemental Figure 5. Mitochondrial Morphology Is Normal in the Root Cells of *miro2* Mutants.

Supplemental Figure 6. Disruption of the Cytoskeleton in Pollen by Cytoskeletal Inhibitors.

Supplemental Figure 7. *MIRO1* cDNA under the Control of Its Endogenous Promoter Restores Normal Mitochondrial Morphology in *miro1* Mutant Pollen.

Supplemental Table 1. Segregation Analysis of the Heterozygous *miro2* Mutants.

Supplemental Movie 1. Mitochondrial Movement in Wild-Type Pollen.

Supplemental Movie 2. Mitochondrial Movement in a *miro1* Mutant Pollen Tube.

Supplemental Movie 3. Mitochondrial Movement Is Arrested in Wild-Type Pollen Treated with Latrunculin B.

Supplemental Movie 4. Mitochondrial Movement Is Arrested in Wild-Type Pollen Treated with Cytochalasin D.

Supplemental Movie 5. Mitochondrial Movement in Wild-Type Pollen Treated with Oryzalin.

Supplemental Movie 6. Mitochondrial Movement in Wild-Type Pollen Treated with Nocodazole.

Supplemental Movie 7. Mitochondrial Movement Is Arrested in *miro1* Mutant Pollen Treated with Latrunculin B.

Supplemental Movie 8. Mitochondrial Movement Is Arrested in *miro1* Mutant Pollen Treated with Cytochalasin D.

Supplemental Movie 9. Mitochondrial Movement in *miro1* Mutant Pollen Treated with Oryzalin.

Supplemental Movie 10. Mitochondrial Movement in *miro1* Mutant Pollen Treated with Nocodazole.

Supplemental Movie 11. Mitochondrial Movement in Wild-Type Pollen Treated with DMSO.

Supplemental Movie 12. Mitochondrial Movement in *miro1* Mutant Pollen Treated with DMSO.

Supplemental Methods. Visualization of the Cytoskeleton in Pollen.

ACKNOWLEDGMENTS

We thank Hugh Dickinson for assistance and advice on electron microscopy and discussion; Ian Moore, Ooi-kock Teh, Marketa Samalova, and Luisa Camacho for assistance and advice on confocal microscopy; Liza A. Pon for critical reading of the manuscript; Jill Harrison for advice; the SeedGenes Project for providing *emb2473* seeds; David Twell for providing pLAT52-TEVL GFP plasmid; Sarah Rogers and Megumi Yamaoka for technical assistance; John Baker for image processing; Kentaro Tamura for actin staining and discussion; Takashi Hashimoto and Shin-ichiro Komaki for microtubule staining; and Haruko Okamoto, Miho Takemura, Keiji Nishida, and Kimitsune Ishizaki for discussion.

Received September 20, 2007; revised January 19, 2008; accepted February 29, 2008; published March 14, 2008.

REFERENCES

Alexander, C., Votruba, M., Pesch, U.E.A., Thiselton, D.L., Mayer, S., Moore, A., Rodriguez, M., Kellner, U., Leo-Kottler, B., Auburger, G., Bhattacharya, S.S., and Wissinger, B. (2000). OPA1, encoding a dynamin-like GTPase, is mutated in autosomal dominant optic atrophy linked to chromosome 3q28. Nat. Genet. **26:** 211–215.

Alonso, J.M., et al. (2003). Genome-wide insertional mutagenesis of *Arabidopsis thaliana.* Science **301:** 653–657.

Altschul, S.F., Madden, T.L., Schäffer, A.A., Zhang, J., Zhang, Z., Miller, W., and Lipman, D.J. (1997). Gapped BLAST and PSI-BLAST: A new generation of protein database search programs. Nucleic Acids Res. **25:** 3389–3402.

Arabidopsis Genome Initiative (2000). Analysis of the genome sequence of the flowering plant *Arabidopsis thaliana.* Nature **408:** 796–815.

Arimura, S., Aida, G.P., Fujimoto, M., Nakazono, M., and Tsutsumi, N. (2004a). *Arabidopsis* dynamin-like protein 2a (ADL2a), like ADL2b,

is involved in plant mitochondrial division. Plant Cell Physiol. **45:** 236–242.

Arimura, S., and Tsutsumi, N. (2002). A dynamin-like protein (ADL2b), rather than FtsZ, is involved in *Arabidopsis* mitochondrial division. Proc. Natl. Acad. Sci. USA **99:** 5727–5731.

Arimura, S., Yamamoto, J., Aida, G.P., Nakazono, M., and Tsutsumi, N. (2004b). Frequent fusion and fission of plant mitochondria with unequal nucleoid distribution. Proc. Natl. Acad. Sci. USA **101:** 7805–7808.

Armstrong, A.F., Logan, D.C., Tobin, A.K., O'Toole, P., and Atkin, O.K. (2006). Heterogeneity of plant mitochondrial responses underpinning respiratory acclimation to the cold in *Arabidopsis thaliana* leaves. Plant Cell Environ. **29:** 940–949.

Barr, C.M., Neiman, M., and Taylor, D.R. (2005). Inheritance and recombination of mitochondrial genomes in plants, fungi and animals. New Phytol. **168:** 39–50.

Batoko, H., Zheng, H.-Q., Hawes, C., and Moore, I. (2000). A Rab1 GTPase is required for transport between the endoplasmic reticulum and Golgi apparatus and for normal Golgi movement in plants. Plant Cell **12:** 2201–2217.

Boldogh, I.R., and Pon, L.A. (2006). Interactions of mitochondria with the actin cytoskeleton. Biochim. Biophys. Acta **1763:** 450–462.

Boldogh, I.R., and Pon, L.A. (2007). Mitochondria on the move. Trends Cell Biol. **17:** 502–510.

Brickley, K., Smith, M.J., Beck, M., and Stephenson, F.A. (2005). GRIF-1 and OIP106, members of a novel gene family of coiled-coil domain proteins: Association *in vivo* and *in vitro* with kinesin. J. Biol. Chem. **280:** 14723–14732.

Chan, D.C. (2006a). Mitochondria: Dynamic organelles in disease, aging and development. Cell **125:** 1241–1252.

Chan, D.C. (2006b). Mitochondrial fusion and fission in mammals. Annu. Rev. Cell Dev. Biol. **22:** 79–99.

Chen, H., Detmer, S.A., Ewald, A.J., Griffin, E.E., Fraser, S.E., and Chan, D.C. (2003). Mitofusins Mfn1 and Mfn2 coordinately regulate mitochondrial fusion and are essential for embryonic development. J. Cell Biol. **160:** 189–200.

Clough, S.J., and Bent, A.F. (1998). Floral dip: A simplified method for *Agrobacterium*-mediated transformation of *Arabidopsis thaliana.* Plant J. **16:** 735–743.

Delettre, C., et al. (2000). Nuclear gene *OPA1*, encoding a mitochondrial dynamin-related protein, is mutated in dominant optic atrophy. Nat. Genet. **26:** 207–210.

Fan, L.-M., Wang, Y.-F., Wang, H., and Wu, W.-H. (2001). *In vitro Arabidopsis* pollen germination and characterization of the inward potassium currents in *Arabidopsis* pollen grain protoplasts. J. Exp. Bot. **52:** 1603–1614.

Fransson, Å., Ruusala, A., and Aspenström, P. (2003). Atypical Rho GTPases have roles in mitochondrial homeostasis and apoptosis. J. Biol. Chem. **278:** 6495–6502.

Fransson, Å., Ruusala, A., and Aspenström, P. (2006). The atypical Rho GTPases Miro-1 and Miro-2 have essential roles in mitochondrial trafficking. Biochem. Biophys. Res. Commun. **344:** 500–510.

Frederick, R.L., McCaffery, J.M., Cunningham, K.W., Okamoto, K., and Shaw, J.M. (2004). Yeast Miro GTPase, Gem1p, regulates mitochondrial morphology via a novel pathway. J. Cell Biol. **167:** 87–98.

Frederick, R.L., and Shaw, J.M. (2007). Moving mitochondria: Establishing distribution of an essential organelle. Traffic **8:** 1668–1675.

Fujimoto, M., Arimura, S., Nakazono, M., and Tsutsumi, N. (2004). A rice dynamin-like protein, OsDRP3A, is involved in mitochondrial fission. Breed. Sci. **54:** 367–372.

Glater, E.E., Megeath, L.J., Stowers, R.S., and Schwarz, T.L. (2006). Axonal transport of mitochondria requires milton to recruit kinesin heavy chain and is light chain independent. J. Cell Biol. **173:** 545–557.

Guo, X., Macleod, G.T., Wellington, A., Hu, F., Panchumarthi, S., Schoenfield, M., Martin, L., Charlton, M.P., Atwood, H.L., and Zinsmaier, K.E. (2005). The GTPase dMiro is required for axonal transport of mitochondria to *Drosophila* synapses. Neuron **47:** 379–393.

Hollenbeck, P.J. (1996). The pattern and mechanism of mitochondrial transport in axons. Front. Biosci. **1:** 91–116.

Hollenbeck, P.J., and Saxton, W.M. (2005). The axonal transport of mitochondria. J. Cell Sci. **118:** 5411–5419.

Howden, R., Park, S.K., Moore, J.M., Orme, J., Grossniklaus, U., and Twell, D. (1998). Selection of T-DNA-tagged male and female gametophytic mutants by segregation distortion in Arabidopsis. Genetics **149:** 621–631.

Karimi, M., De Meyer, B., and Hilson, P. (2005). Modular cloning in plant cells. Trends Plant Sci. **10:** 103–105.

Krichevsky, A., Kozlovsky, S.V., Tian, G.-W., Chen, M.-H., Zaltsman, A., and Citovsky, V. (2007). How pollen tubes grow. Dev. Biol. **303:** 405–420.

Logan, D.C. (2006a). The mitochondrial compartment. J. Exp. Bot. **57:** 1225–1243.

Logan, D.C. (2006b). Plant mitochondrial dynamics. Biochim. Biophys. Acta **1763:** 430–441.

Logan, D.C., and Leaver, C.J. (2000). Mitochondria-targeted GFP highlights the heterogeneity of mitochondrial shape, size and movement within living plant cells. J. Exp. Bot. **51:** 865–871.

Logan, D.C., Scott, I., and Tobin, A.K. (2004). ADL2a, like ADL2b, is involved in the control of higher plant mitochondrial morphology. J. Exp. Bot. **55:** 783–785.

Lovy-Wheeler, A., Cárdenas, L., Kunkel, J.G., and Hepler, P.K. (2007). Differential organelle movement on the actin cytoskeleton in lily pollen tubes. Cell Motil. Cytoskeleton **64:** 217–232.

Mansfield, S.G., and Briarty, L.G. (1990). Early embryogenesis in *Arabidopsis thaliana.* II. The developing embryo. Can. J. Bot. **69:** 461–476.

McBride, H.M., Neuspiel, M., and Wasiak, S. (2006). Mitochondria: More than just a powerhouse. Curr. Biol. **16:** R551–R560.

McElver, J., et al. (2001). Insertional mutagenesis of genes required for seed development in *Arabidopsis thaliana.* Genetics **159:** 1751–1763.

Meinke, D.W. (1982). Embryo-lethal mutants of *Arabidopsis thaliana*: Evidence for gametophytic expression of the mutant genes. Theor. Appl. Genet. **63:** 381–386.

Neff, M.M., Neff, J.D., Chory, J., and Pepper, A.E. (1998). dCAPS, a simple technique for the genetic analysis of single nucleotide polymorphisms: Experimental applications in *Arabidopsis thaliana* genetics. Plant J. **14:** 387–392.

Okamoto, K., and Shaw, J.M. (2005). Mitochondrial morphology and dynamics in yeast and multicellular eukaryotes. Annu. Rev. Genet. **39:** 503–536.

Parton, R.M., Fischer-Parton, S., Trewavas, A.J., and Watahiki, M.K. (2003). Pollen tubes exhibit regular periodic membrane trafficking events in the absence of apical extension. J. Cell Sci. **116:** 2707–2719.

Preuss, D., Rhee, S.Y., and Davis, R.W. (1994). Tetrad analysis possible in *Arabidopsis* with mutation of the QUARTET (QRT) genes. Science **264:** 1458–1460.

Rice, S.E., and Gelfand, V.I. (2006). Paradigm lost: milton connects kinesin heavy chain to miro on mitochondria. J. Cell Biol. **173:** 459–461.

Shan, Y., Hexige, S., Guo, Z., Wan, B., Chen, K., Chen, X., Ma, L., Huang, C., Zhao, S., and Yu, L. (2004). Cloning and characterization of the mouse *Arht2* gene which encodes a putative atypical GTPase. Cytogenet. Genome Res. **106:** 91–97.

Sheahan, M.B., McCurdy, D.W., and Rose, R.J. (2005). Mitochondria as a connected population: Ensuring continuity of the mitochondrial

genome during plant cell dedifferentiation through massive mitochondrial fusion. Plant J. **44:** 744–755.

Sheahan, M.B., Rose, R.J., and McCurdy, D.W. (2004). Organelle inheritance in plant cell division: The actin cytoskeleton is required for unbiased inheritance of chloroplasts, mitochondria and endoplasmic reticulum in dividing protoplasts. Plant J. **37:** 379–390.

Stickens, D., and Verbelen, J.-P. (1996). Spatial structure of mitochondria and ER denotes changes in cell physiology of cultured tobacco protoplasts. Plant J. **9:** 85–92.

Stowers, R.S., Megeath, L.J., Górska-Andrzejak, J., Meinertzhagen, I.A., and Schwarz, T.L. (2002). Axonal transport of mitochondria to synapses depends on milton, a novel *Drosophila* protein. Neuron **36:** 1063–1077.

Thompson, J.D., Higgins, D.G., and Gibson, T.J. (1994). CLUSTAL W: Improving the sensitivity of progressive multiple sequence alignment through sequence weighting, position-specific gap penalties and weight matrix choice. Nucleic Acids Res. **22:** 4673–4680.

Twell, D., Yamaguchi, J., and McCormick, S. (1990). Pollen-specific gene expression in transgenic plants: Coordinate regulation of two different tomato gene promoters during microsporogenesis. Development **109:** 705–713.

Tzafrir, I., Pena-Muralla, R., Dickerman, A., Berg, M., Rogers, R., Hutchens, S., Sweeney, T.C., McElver, J., Aux, G., Patton, G., and Meinke, D. (2004). Identification of genes required for embryo development in Arabidopsis. Plant Physiol. **135:** 1206–1220.

Van Gestel, K., Köhler, R.H., and Verbelen, J.-P. (2002). Plant mitochondria move on F-actin, but their positioning in the cortical cytoplasm depends on both F-actin and microtubules. J. Exp. Bot. **53:** 659–667.

Yadegari, R., de Paiva, G.R., Laux, T., Koltunow, A.M., Apuya, N., Zimmerman, J.L., Fischer, R.L., Harada, J.J., and Goldberg, R.B. (1994). Cell differentiation and morphogenesis are uncoupled in Arabidopsis *raspberry* embryos. Plant Cell **6:** 1713–1729.

Yaffe, M.P. (1999). The machinery of mitochondrial inheritance and behavior. Science **283:** 1493–1497.

Yang, S., Sweetman, J.P., Amirsadeghi, S., Barghshi, M., Huttly, A.K., Chung, W.-I., and Twell, D. (2001). Novel anther-specific *myb* genes from tobacco as putative regulators of phenylalanine ammonia-lyase expression. Plant Physiol. **126:** 1738–1753.

Yoshinaga, K., Arimura, S., Niwa, Y., Tsutsumi, N., Uchimiya, H., and Kawai-Yamada, M. (2005). Mitochondrial behaviour in the early stages of ROS stress leading to cell death in *Arabidopsis thaliana.* Ann. Bot. (Lond.) **96:** 337–342.

Zimmermann, P., Hirsch-Hoffmann, M., Henning, L., and Gruissem, W. (2004). GENEVESTIGATOR. Arabidopsis microarray database and analysis toolbox. Plant Physiol. **136:** 2621–2632.

Zottini, M., Barizza, E., Bastianelli, F., Carimi, F., and Lo Schiavo, F. (2006). Growth and senescence of *Medicago truncatula* cultured cells are associated with characteristic mitochondrial morphology. New Phytol. **172:** 239–247.

Züchner, S., et al. (2004). Mutations in the mitochondrial GTPase mitofusin 2 cause Charcot-Marie-Tooth neuropathy type 2A. Nat. Genet. **36:** 449–451.